A Review of the Geological Constraints on the Conductive Boundary Layer at the Base of the Hydrothermal System at Mid-Ocean Ridges

K.M. Gillis and L.A. Coogan

2018

Geochemistry, Geophysics, Geosystems

RESEARCH ARTICLE
10.1029/2018GC007878

A Review of the Geological Constraints on the Conductive Boundary Layer at the Base of the Hydrothermal System at Mid-Ocean Ridges

K. M. Gillis[1] and L. A. Coogan[1]

[1]School of Earth and Ocean Sciences, University of Victoria, Victoria, British Columbia, Canada

Key Points:
- Low permeability paleoconductive boundary layers record peak recrystallization temperatures of >900 °C, ductile behavior, and partial melting
- Heat fluxes derived from paleothermal gradients and steady state magmatic construction calculations are much less than those of active vent sites
- Thin conductive boundary layers form by disaggregation, stoping, and assimilation of altered upper crust during magmatic advance

Supporting Information:
- Supporting Information S1
- Data Set S1
- Data Set S2

Correspondence to:
K. M. Gillis,
kgillis@uvic.ca

Citation:
Gillis, K. M., & Coogan, L. A. (2019). A review of the geological constraints on the conductive boundary layer at the base of the hydrothermal system at mid-ocean ridges. *Geochemistry, Geophysics, Geosystems*, *20*. https://doi.org/10.1029/2018GC007878

Received 2 AUG 2018
Accepted 6 DEC 2018
Accepted article online 11 DEC 2018

Abstract Models of high-temperature hydrothermal systems at intermediate- to fast-spreading mid-ocean ridges have a conductive boundary layer (CBL) separating the magmatic heat source from the convecting hydrothermal fluid. Paleo-CBLs preserved in the geological record provide a means to test theoretical models of the thermal, mechanical, and petrological evolution of this boundary. CBLs occur as metamorphic contact aureoles at or near the dike-gabbro boundary where axial magma lenses (now plutonic rocks) intruded into the basal dikes, leading to their transformation into low permeability granulite and hornblende hornfels at >800 °C. Paleo-CBLs are well documented in the Troodos and Oman ophiolites, and evidence of similar lithologies has been found at every location where the dike-gabbro transition has been mapped and/or sampled in modern fast-spreading crust (Hess and Pito Deeps, IODP Hole 1256D). Evaluation of the geothermometers used in studies of the thermal evolution of the CBL shows a lack of consistency that can be understood in terms of compositional controls. Peak temperatures are >900 °C in all areas at the base of the CBL, leading to partial melting, stoping, and disaggregation that facilitates thinning from below as required to maintain the high heat fluxes necessary to drive active black smoker systems. However, such thin CBLs are not the norm; steady state conditions must have thicker CBLs and smaller heat fluxes. In turn, global estimates of properties such as chemical fluxes for normal hydrothermal conditions may lead to substantially different element/heat fluxes than those based on active systems.

1. Introduction

The roof zone of axial magma lenses (AMLs) along the global mid-ocean ridge (MOR) system plays a significant role in the evolution of magmatic and hydrothermal systems. These systems are separated by a conductive boundary layer (CBL; also called the thermal boundary layer) across which heat is transferred from the magma to the hydrothermal fluid. The heat flux across this boundary layer controls the rate of crystallization in the AML and hence plays an important role in magma dynamics, lower crustal accretion and mid-ocean ridge basalt (MORB) differentiation. Likewise, the heat flux across the CBL controls the fluid flux into the overlying hydrothermal system. While the CBL is expected to be dynamic, evolving in response to processes such as AML replenishment and dike emplacement, theoretical models treat this boundary as a static boundary layer separating two convecting regions (Figure 1).

Early theoretical models of high-temperature oceanic hydrothermal systems predicted the presence of an impermeable boundary layer, separating a magmatic heat source from convecting hydrothermal fluid, across which heat is conducted (e.g., Cann et al., 1985; Lister, 1983; Lowell & Burnell, 1991). These and other studies showed that in order to maintain a high heat flux, CBLs would need to be thin (few tens of meters), with steep thermal gradients bounded by magma temperatures at its base and ambient hydrothermal temperatures at its top (e.g., Lowell & Burnell, 1991; Lowell & Germanovich, 1994). The CBL thickness is proportional to the heat flux across it, such that when CBLs are thin heat fluxes are high and heat fluxes diminish as the CBL thickens (e.g., Lowell & Germanovich, 1994; Lowell & Germanovich, 2004). There is much interest in understanding the processes by which the CBL remains thin because heat flux is linked to the vigor and temperature of hydrothermal vent sites. Two general models have emerged: the first invokes a cracking front that taps heat by cracks migrating downward into the top of the CBL (e.g., Lister, 1974, 1983) and the second requires replenishment of the magmatic heat source keeping the base of the CBL from thickening downward (e.g., Lowell & Germanovich, 1994). It is now generally accepted that the latter model is a better representation of magma-rich environments such as fast-spreading ridges, whereas the former model may be appropriate for some magma-poor settings (Olive & Crone, 2018; Wilcock & Delaney,

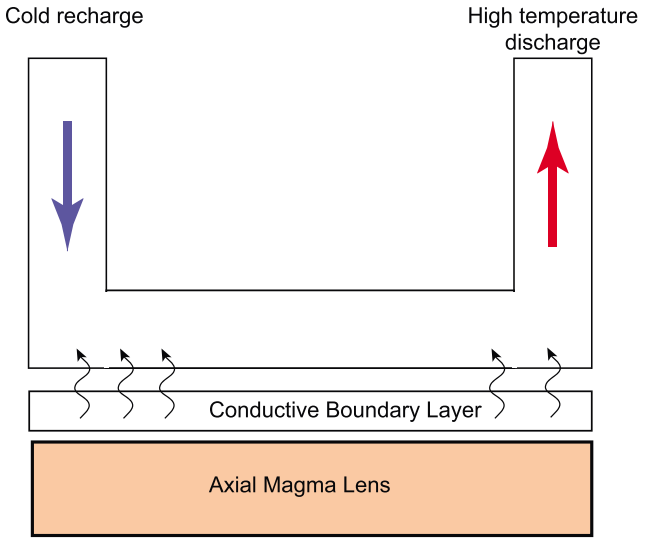

Figure 1. Schematic of the simple, static, single pass model for mid-ocean ridge hydrothermal systems (e.g., Strens & Cann 1982; Lowell & Germanovich, 1994; Lowell et al., 2013). Cold recharging fluids flow down through the permeable upper crust. Heat from the axial magma lens is conductively transported across a thin (~<50 m) conductive boundary layer into the base of the circulating hydrothermal system hosted in the sheeted dike complex. Fluids are heated, and the hot buoyant fluids ascend to the seafloor.

1996). More recent models have explored how hydrothermal cooling effects the evolution of AMLs and how episodic replenishment of AMLs impacts heat transfer into the hydrothermal system (e.g., Fontaine et al., 2011; Liu & Lowell, 2009).

The presence of CBLs at the magma-hydrothermal boundary was first confirmed by geological studies in the Troodos ophiolite where a regionally extensive, thin, metamorphic contact aureole centred at the sheeted dike-gabbro boundary was discovered (Gillis & Roberts, 1999). With a sharp intrusive boundary at its base, previously hydrated basal sheeted dikes were recrystallized at high temperatures (>800 °C) over a narrow (<30 m) distance, creating an impermeable horizon. Within a decade of these observations, thin contact aureoles and high-temperature metamorphic rocks characteristic of CBL conditions were documented along the dike-gabbro boundary in the Oman ophiolite (France et al., 2009; Gillis, 2008) and modern, fast-spreading Pacific ocean crust in the three locations where the dike-gabbro boundary has been investigated/sampled (e.g., France et al., 2009; Gillis, 2008; Koepke et al., 2008; Wilson et al., 2006). While this distribution confirms that CBLs are a fundamental feature of accretionary processes at intermediate- to fast-spreading MORs, they are not expected to be preserved everywhere at the dike-gabbro transition. This is because paleo-CBLs typically record the last intrusive event, meaning paleo-CBL preservation would depend on the nature of the final phase of magmatism at a given location (Nicolas et al., 2008).

Geophysical studies have also identified regions with physical properties consistent with those of CBLs in the vicinity of AMLs at intermediate- to fast-spreading MORs. These consist of ~50- to 200-m thick zones with higher than expected seismic velocities immediately overlying some AMLs. The high velocities are interpreted as suggesting lower permeability than in the overlying dikes (Marjanovic et al., 2017; Singh et al., 1999). In some places, microearthquakes appear to occur within the high velocity regions (Tolstoy et al., 2008; Waldhauser & Tolstoy, 2011), suggesting a very thin CBL or a temporal perturbation of it. Other high velocity regions lack microearthquakes and have been interpreted as places where hydrothermal sealing has reduced crustal permeability, thickening the CBL, and thus limiting hydrothermal cooling (Arnoux et al., 2017; Weekly et al., 2014). In other areas low-velocity zones are also observed overlying AMLs, suggesting a thin CBL (Arnoux et al., 2017; Wilcock et al., 2009). These geophysical approaches provide a temporal snapshot of the magma-hydrothermal system, although with poor spatial resolution compared to geological studies.

In the two decades since conductive boundary layers associated with oceanic magma-hydrothermal systems were confirmed in the geological record (Gillis & Roberts, 1999) and high seismic velocity zones were geophysically imaged at the roof of the AML at a modern MOR (Singh et al., 1999), there has been significant interest to better understand this fundamental boundary. In this contribution we review and synthesize new and published geological constraints on the thermal history and petrological evolution of CBLs preserved in metamorphic contact aureoles. With this perspective, we then examine the thermal and mechanical evolution of this dynamic boundary and the processes that control its thickness and hence the heat fluxes across it. In this context we present a conceptual model for the magma-hydrothermal transition at intermediate- to fast-spreading mid-ocean ridges. The perspective taken bears on the evolution of AML magmas and their contamination by assimilation of hydrothermally altered lower dikes; however, a thorough analysis of these processes is out of the scope of this contribution. In the following text, we use the terms CBL and contact aureole as follows. We use conductive boundary layer to refer to the concept of a boundary layer between a magma chamber and hydrothermal system across which heat transport is largely conductive—of course in nature things are more complicated. Contact aureole refers to a zone of prograde metamorphic rock, with low permeability, that records a steep thermal gradient between underlying plutonic rocks and overlying hydrothermally altered dikes that formed in and around a paleo-CBL.

2. The Geology of the Magma-Hydrothermal Transition

Our knowledge of the geological characteristics of the magma-hydrothermal transition, and the CBL in particular, comes from field relationships along the sheeted dike-gabbro transition in ophiolites, and petrological constraints from samples from this boundary from ophiolites and young, fast-spreading ocean crust recovered by submersible and drilling (Table S1). The key relationships are summarized here; readers are directed to the original references for more detail.

2.1. Study Areas: Where Have Rocks From the CBL Been Found?

The best spatial constraints on the nature of the CBL come from two well studied ophiolites: the Troodos ophiolite, Cyprus, where there is a well exposed, regionally extensive (>3 km) contact aureole at the dike-gabbro transition in the Platanistasa area (Gillis & Coogan, 2002; Gillis & Roberts, 1999; this study) and the Oman ophiolite, where three discontinuous exposures (<500-m wide) of the dike-gabbro boundary in the Wadi Tayin Massif have been studied (Wadi Gideah and Ahamadi Hills, France et al., 2009; Hiim, Gillis, 2008). These ophiolite studies are complemented by samples from young, fast-spreading Pacific crust recovered by submersible and ROV in the vicinity of well-exposed dike-gabbro boundaries at Hess and Pito Deeps (Gillis, 2008; this study) and drill core from the dike-gabbro boundary at IODP Hole 1256D (France et al., 2009; Koepke et al., 2008; Teagle et al., 2006; Teagle et al., 2012; Wilson et al., 2006). Spatial relationships in these study areas are less well constrained than for the ophiolites due to absence of detailed sampling in the tectonic exposures (Gillis, 2008) and the very low recovery (<7%) within the lowermost sheeted dikes at Hole 1256D (Teagle et al., 2006). Indeed, in some cases it is not possible to determine if samples of recrystallized dikes come from a contact aureole or are xenoliths.

2.2. Geological Relationships Near the Magma-Hydrothermal Transition

The base of the sheeted dike complex at intermediate- to fast-spreading ridges is commonly marked by complex intrusive relationships, where in the simplest form, gabbros intrude into dikes or dikes intrude either laterally (i.e., along axis) or vertically (i.e., from deeper in the crust) into preexisting gabbros (e.g., Karson, 2002; Nicolas & Boudier, 1991; Pedersen, 1986). Either of these simple forms may dominate on lateral length scales of tens of meters to kilometers along this boundary (e.g., Malpas, 1990; Pallister & Hopson, 1981; Pedersen, 1986; Rothery, 1983). The uppermost plutonics (typically within ~1 km of the dikes) contain xenoliths of hydrothermally altered dikes and, more rarely, other plutonic rocks. The isotopic composition of these xenoliths point to high temperature exchange with hydrothermal fluids prior to their being stoped into the AML (Gregory & Taylor, 1981; Kirchner & Gillis, 2012; Stakes & Taylor, 1992). Xenoliths have sharp to diffuse external boundaries (Figure 2f; see also Figures 4, 6, and 8 in France et al., 2009), implying they can undergo dissolution and/or partial melting. These observations are consistent with the strong overenrichment of Cl in MORB from intermediate- to fast-spreading ridges that suggests assimilation of seawater-derived components (brine inclusions, altered rocks) into the AML prior to eruption (Michael & Schilling, 1989; Michael & Cornell, 1998; le Roux et al., 2006). The upper gabbros have compositions and textures that reflect the mixing and crystallization of mantle-derived magmas influenced by the assimilation of altered upper crust (e.g., France et al., 2013; Gillis et al., 2003; Malpas, 1990; Zhang, Koepke, France, & Godard, 2017). Collectively, these relationships point to a dynamic boundary at the base of the CBL that reflects the waxing and waning of the magmatic system at (or near) a spreading axis.

The clearest records of the conditions within the CBL come from locations where the last magmatic event was shallow-level replenishment or intrusion, that is, where gabbros intrude into the base of the sheeted dikes (Figure 2e). Here the lowermost dikes (±gabbros) are recrystallized into very fine grained metamorphic rocks called hornfels that are typical of contact aureoles in all geological settings. Deeper-level replenishment or intrusion can lead to hornfelsic dikes and hornfelsic gabbros within the plutonic sequence (i.e., below the sheeted dike-gabbro boundary), but the top and bottom of the associated aureoles are difficult to identify in ophiolites. In addition, contact aureoles centred at the dike-gabbro boundary may be cut by later dikes intruding either from depth or laterally, resulting in a complex juxtapositioning of hornfelsic and nonhornfelsic dikes. Hence, we focus on clear intrusive relationships where the top of the plutonics intrudes the base of the dikes (Figure 2).

The studied contact aureoles share many common characteristics. The thickness of hornfelsic aureoles in the Troodos and Oman ophiolites are <30 and <50 m, respectively (France et al., 2009; Gillis, 2008; Gillis &

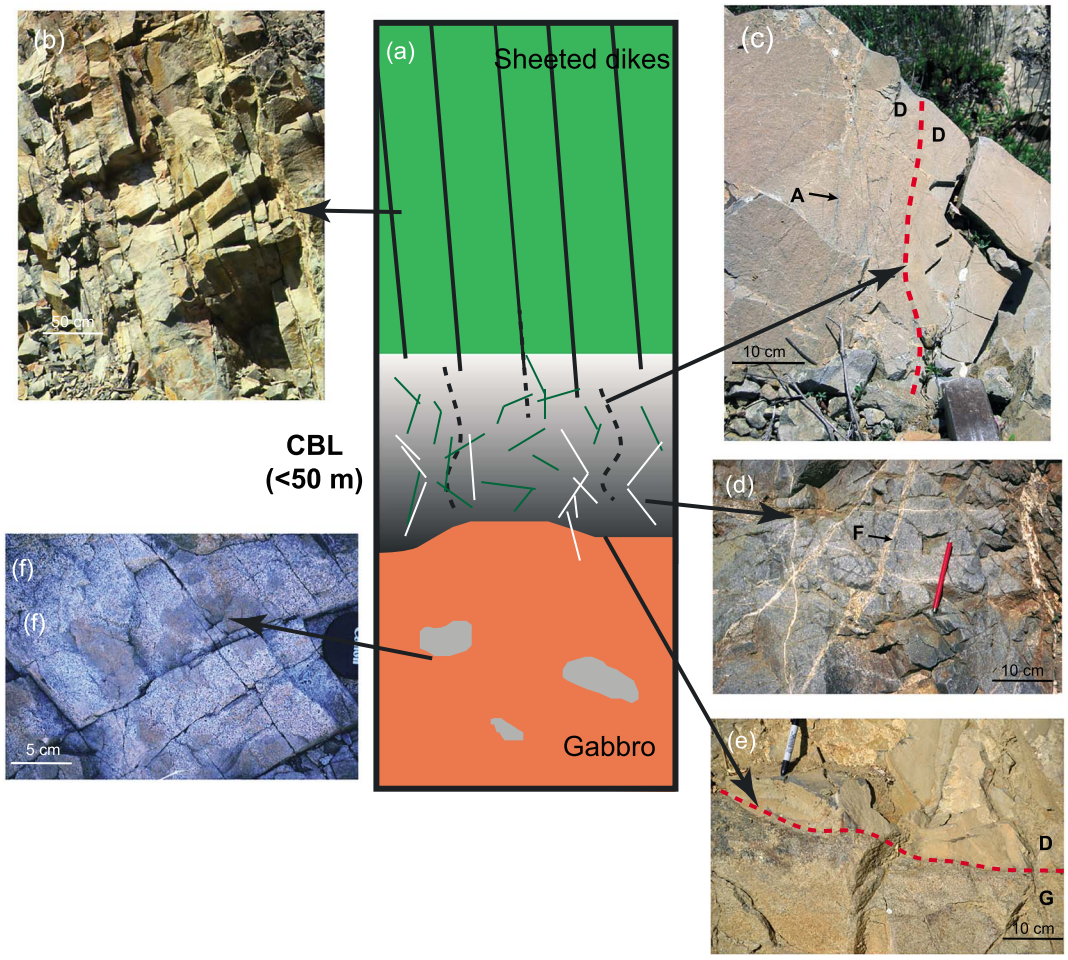

Figure 2. (a) Schematic diagram showing the geological relationships in the vicinity of a paleoconductive boundary layer (CBL) showing a sharp intrusive boundary at the base of the CBL. Within the CBL cooling fractures are annealed and dike margins are locally sinuous, suggesting the rocks were ductile at peak temperatures. Amphibole (green) and felsic (white) vein networks locally cut the hornfels. The underlying gabbro contains xenoliths of altered dikes. Outcrop photos of key elements: (b) sheeted dikes above the CBL, note well developed, parallel cooling fractures; (c) sinuous, annealed dike margin (red dashed line) within the contact aureole, suggesting that the rocks were ductile at peak temperatures; slightly different colors across the boundary reflect different grain size of adjacent dikes; dikes contain amphibole vein network; (d) felsic vein network in hornfels, formed by partial melting of the CBL; (e) sharp intrusive contact, gabbro intrudes dikes (red dashed line); (f) hornfelsic xenoliths within the uppermost gabbros. Abbreviations: G = gabbro, D = dike, A = amphibole vein, F = felsic vein.

Roberts, 1999) and at Hole 1256D ~60 m (Wilson et al., 2006), although with the very low recovery this is not well constrained. Hornfelsic rocks that comprise the contact aureoles are massive and indurated (Figure 2c), lack the cooling fractures typical of sheeted dikes (Figure 2b), and have undergone significant grain size reduction (compare Figures 3a and 3b). Collectively, these features indicate significantly lower permeability than found in the overlying dikes that host the hydrothermal system. Dike margins are annealed and can be swirly (Figure 2c), in that their orientation deviates smoothly on decimeter length scales from the regional strike of the dikes. This indicates the CBL was, at least at times, ductile although there is no microscopic evidence of crystal plastic deformation. Outcrops may contain felsic lithlogies (diorite to tonalite) in the form of centimeter-scale veins, centimeter- to decimeter-scale patches to larger zones whose distribution is commonly discontinuous across an outcrop. In the Troodos ophiolite these are focused in the lower half of the aureole (Figure 2d; see also Figure 1 in Gillis & Coogan, 2002). Such felsic rocks are interpreted as partial melts of the surrounding rocks (e.g., France et al., 2010; Gillis & Coogan, 2002). Their relatively coarse grain size, despite their small size, indicates the veins intruded while the host dikes were very hot. Near the upper boundaries of the aureoles, outcrops become progressively more fractured upward and samples show a

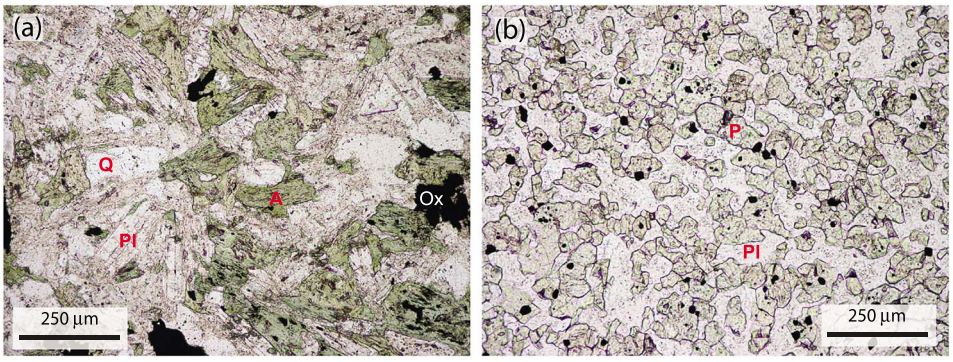

Figure 3. Photomicrographs of: (a) typical fine grained, hydrothermally altered dike with fibrous amphibole completely replacing clinopyroxene, albite and chlorite partially replacing plagioclase, and trace titanite replaces Fe-Ti oxides; original diabasic texture is preserved (sample 2012CL39); and (b) classic granulite hornfels with very fine grained equidimensional, granoblastic assemblage of plagioclase and pyroxene (clinopyroxene ≫orthopyroxene) and discrete interstitial ilmenite and magnetite (black; sample 2011KG18; complete recrystallization). Plain polarized light. Abbreviations: Pl = plagioclase; P = pyroxene; A = amphibole; Ox = Fe-Ti oxide. Both samples from the Platanistasa contact aureole, near the village of Livadia.

decrease in the extent of recrystallization associated with prograde metamorphism, suggesting slightly higher permeability and cooler conditions.

Amphibole or pyroxene veins locally cut the contact aureole, the latter being interpreted as earlier formed amphibole veins that have been recrystallized during prograde metamorphism (France et al., 2009; Gillis, 2008; Gillis & Roberts, 1999). Amphibole veins record the cracking of the aureole and the penetration of hydrothermal fluids into the cracks prior to their sealing. In the Troodos ophiolite aureole, amphibole veins are cut by felsic veins, and vice versa. These cross-cutting relationships, and the occurrence of pyroxene veins that represent reheated amphibole veins, suggest that (i) the temperature in the aureole can vary substantially and (ii) cracking from below and partial melting of the CBL (forming felsic veins) and cracking from above (forming amphibole veins) occurred while the magmatic system was active.

2.3. Rock Types that Comprise the CBL

2.3.1. Protoliths: The Rocks that Become the CBL

Field relations show that the hornfelsic contact aureoles grade upward into the lower sheeted dikes and the hornfels closest to the upper margin of the aureoles preserve relict igneous textures identical to those in the adjacent hydrothermally altered lower dikes. These observations indicate the protoliths were hydrated dikes (± gabbros) initially altered at temperatures (~400° to 550 °C), typical of alteration conditions found in the lower sheeted dike complexes and inferred for the base of hydrothermal systems beneath black smokers. This means that the rocks forming the CBL crystallized from a magma, were then hydrothermally altered (i.e., retrograde metamorphism; Figure 3a), and were then reheated by magma advance and recrystallized to a finer grained, less hydrous mineral assemblage (i.e., prograde metamorphism). The retrograde hydrothermal metamorphic assemblages include hydrothermal amphibole + albitized plagioclase ± chlorite ± epidote ± quartz ± titanite and, only in Oman, ± prehnite ± pumpellyite (Alt et al., 2010; France et al., 2009; Gillis et al., 2001; Gillis & Roberts, 1999; Heft et al., 2008; Nehlig et al., 1994). The degree of replacement of the igneous phases (dominantly clinopyroxene and plagioclase) is low (<25%) in the Pacific lower dike suites (Alt et al., 2010; Gillis et al., 2001; Heft et al., 2008) and much higher in the ophiolites where relict igneous clinopyroxene and plagioclase is rare (France et al., 2009; Gillis & Roberts, 1999; Nehlig et al., 1994).

2.3.2. Granulite and Hornblende Hornfels: The Dominant Lithologies of the CBL

Contact metamorphism of the previously hydrothermally altered lower dikes produces a very fine grained rock that is massive and indurated with very low permeability, features consistent with a boundary layer across which heat would be conducted. Recrystallization produces two common rock types. The first is granulite hornfels, with an assemblage of clinopyroxene + plagioclase + orthopyroxene ± amphibole ± quartz + ilmenite + magnetite. This rock type is equivalent to the pyroxene hornfels of Gillis and Roberts (1999) and Gillis (2008) and the granoblastic dikes of Koepke et al. (2008); the name granulite hornfels is used here to emphasize the requirement for two pyroxenes in the mineral assemblage. Classic

granulite hornfels have equidimensional grains of plagioclase and pyroxene that are subequal in size, reflective of complete recrystallization (Figure 3b). Typical granulite hornfels have undergone somewhat less complete recrystallization, such that plagioclase is tabular and slightly coarser grained than associated pyroxene, pyroxene forms discrete grains or aggregates of grains, and the oxide phases occur as inclusions in clinopyroxene or as discrete grains (Figures S1c and S1d). In both the classic and typical granulite hornfels, brown (prograde) amphibole occurs as a minor phase that may be interstitial, poikiolitic with plagioclase and/or clinopyroxene inclusions, or rim pyroxene.

The second, somewhat lower grade, rock type that makes up contact aureoles is hornblende hornfels, comprised of amphibole + plagioclase + clinopyroxene + quartz + ilmenite + magnetite. Textures in hornblende hornfels are far more heterogeneous than those of granulite hornfels (Figures S1e and S1f). At one end of the spectrum, they are texturally similar to the typical granulite hornfels but lack orthopyroxene, and at the other end, <50% of the sample has been recrystallized during prograde metamorphism (i.e., some original diabasic textures are preserved). Prograde brown amphibole may be interstitial, poikiolitic with plagioclase and/or igneous or metamorphic clinopyroxene inclusions, or rim pyroxene. A prograde origin is supported by the observation that granular brown amphibole rims clots of fibrous amphibole replacing clinopyroxene, suggesting formation by recrystallization of fibrous amphibole (see Figure 4b, Gillis & Roberts, 1999). It may also be noted that fibrous amphibole is the dominant texture in the lower dikes. The least recrystallized hornblende hornfels share many features of the hydrothermally altered dikes that have not been thermally metamorphosed (i.e., the protoliths). A key distinction is the presence of prograde metamorphic clinopyroxene in the hornblende hornfels, identified on the basis of being texturally clear (e.g., lacking inclusions) and compositionally depleted in minor elements (Al_2O_3, TiO_2, and Cr_2O_3; e.g., Manning & Bird, 1986). The preservation of some relict retrograde hydrothermal minerals in the hornblende hornfels is readily explained as they typically comprise the outer boundary of the aureole, where the rocks are less indurated and thus, more permeable, and temperatures were lower.

A well-exposed contact aureole in the Troodos ophiolite (Gillis & Roberts, 1999; supporting information Text S1; supporting information Figure S2) provides insight into the distribution of lithologies across a contact aureole in one location. Granulite hornfels make up the lower 50% of the aureole and hornblende hornfels the upper 50%, consistent with higher recrystallization temperatures closer to the underlying plutonic rocks that acted as a heat source (paleomagma chamber; see below). The margins of the aureole have predictable textures, such that classic granulite hornfels are restricted to within 2–4 m of the intrusive contact and hornblende hornfels with the lowest degree of recrystallization mark the upper margin against the background dikes. In between, the aureole is heterogeneous with the degree of recrystallization, mineral textures (e.g., discrete grains or aggregates of pyroxene), and specific mineral assemblages (e.g., presence or absence of amphibole or quartz) varying on a scale of millimeters to decimeters. To some extent, this must reflect heterogeneity in the protolith (e.g., % hydrous minerals), as well as evolving conditions (e.g., H_2O activity).

Insight into the spatial variability in the conditions in the CBL comes from comparison of the lithologies observed in different study areas along with the peak metamorphic temperatures (see below). In the Oman ophiolite, two of the three studied areas lack granulite hornfels and at Hole 1256D hornblende hornfels have not been identified, although some granoblastic samples lacking orthopyroxene may be equivalent (France et al., 2009; Koepke et al., 2008). These variations, while not robust in terms of number of locations, suggest that CBLs may not achieve the same peak conditions everywhere, although we cannot rule out the possibility that these variations reflect different protolith compositions and/or incomplete sampling in some areas.

In all locations, the hornfels are overprinted by later retrograde metamorphism. The amphibolite to greenschist facies assemblages formed during this retrograde metamorphism are typical of those found in associated dikes and gabbroic rocks from each area. The extent of this overprint varies from <5% (e.g., Troodos ophiolite, Hess Deep) to >20% (e.g., Oman ophiolite, Pito Deep, Hole 1256D). This partial overprinting of the prograde metamorphic assemblages developed as the CBLs cooled sufficiently to allow for cracking and ingress of lower temperature hydrothermal fluids. The record of this retrograde metamorphism demonstrates that the rocks were not subsequently reheated; that is, the rocks were no longer part of a CBL as this portion of the crust reached the off-axis edge of the AML or the AML and hence magma-hydrothermal boundary deepened.

2.3.3. Association of Granulite Hornfels With Felsic Lithologies: The CBL Partially Melts

The close spatial association of the hornfels and felsic lithologies in many of the study areas (Troodos and Oman ophiolites, Hole 1256D) suggests that CBLs partially melt and that this is a common process (e.g., France et al., 2009; Gillis & Coogan, 2002; Zhang, Koepke, France, & Godard, 2017). Average peak metamorphic temperatures (see below) are higher than wet basalt solidus temperatures (~850° to <940 °C at 0.1 to 0.2 GPa, e.g., Beard & Lofgren, 1991; Erdmann et al., 2015; France et al., 2010), conditions that could induce partial melting as prograde metamorphism releases water into the system. Comparison of the mineralogy and geochemistry of the natural rocks (felsic lithologies, granulite hornfels) with the products of partial melting experiments suggests that, at least in some cases, the granulite assemblage is the solid residue of partial melting of the hydrothermally altered dikes that produced the felsic melt (e.g., Beard & Lofgren, 1991; Erdmann et al., 2015; France et al., 2010, 2014; Gillis & Coogan, 2002). Modeling of the chemistry of felsic rocks found in the Troodos ophiolite aureole suggests on average ~30% disequilibrium partial melting of the basaltic protolith (Gillis & Coogan, 2002), whereas somewhat lower extents (≤10%) are suggested for samples from the 1256D aureole (France et al., 2013; Zhang, Koepke, France, & Godard, 2017).

2.4. Mineral and Fluid Inclusion Compositions

Most of the phases in both hornfels types may have a metamorphic or igneous origin, and hence, the above discussion relies somewhat on identifying the origin of the different phases. Major and minor element contents can be used to confirm the metamorphic origin of the pyroxenes and plagioclase (e.g., France et al., 2009; Gillis, 2008; Koepke et al., 2008; Manning & Bird, 1986), whereas textures and major and trace element contents are used to assess the origin of amphibole (e.g., Gillis & Coogan, 2002). It is necessary to discuss the origin of amphibole in more detail than the other phases because it may crystallize from a melt, or be formed during either prograde or retrograde metamorphism. Textures combined with trace element data provide the best constraints to distinguish between igneous and metamorphic origins. This is because the lithophile trace element content of a seawater-derived fluid is significantly (orders of magnitude) less than that of a melt formed by either partial melting of the aureole or late stage crystallization of the AML (e.g., Coogan et al., 2001). In some granulite hornfels from the Troodos ophiolite, trace element contents of some brown granular groundmass amphibole indicate crystallization from trapped melt (Gillis & Coogan, 2002). In other granulite hornfels from the Troodos and Oman ophiolites, and Pito Deep, brown granular amphibole rimming pyroxene or forming poikiloblasts are interpreted as part of the peak or near peak metamorphic assemblage (France et al., 2009; Gillis, 2008; Gillis & Roberts, 1999). In IODP Hole 1256D, Koepke et al. (2008) do not include amphibole in the peak metamorphic assemblage as it apparently formed at lower temperatures than coexisting pyroxenes; however, as discussed below, this temperature difference is probably an artifact of the amphibole thermometry (see section 3.1).

A record of the behavior of volatiles in the AML is preserved in hydrous mineral compositions and fluid inclusions in the upper plutonics. Boron systematics in magmatic amphibole from Hess Deep suggest that magma degassing occurs during the latter stages of AML crystallization (Gillis et al., 2003). Evidence for degassing is also recorded in magmatic apatite from Hess Deep (Gillis et al., 2003), Oman (supporting information Figure S3), and ODP Hole 1256D (Zhang, Koepke, Albrecht, et al., 2017), which show a negative correlation between their Cl and F contents, with more Cl-rich apatite being hosted in less evolved lithologies (gabbros) than F-rich apatite (tonalities). While Cl-systematics are complicated, one interpretation of this trend is that Cl is partitioned into the fluid phase as magmas crystallize and degas, thus increasing the F/Cl in the residual magma and hence later stage apatite (Gillis et al., 2003). Fluid inclusions hosted in evolved plutonic rocks from four of the field areas also show that magmatic fluids are exsolved as supercritical brines, or vapors + brines (Alt et al., 2010; Juteau et al., 2000; Kelley et al., 1992; Kelley & Malpas, 1996; Nehlig, 1991). Similarly, fluid inclusions hosted in felsic lithologies near the dike-gabbro boundary suggest the presence of brines (Alt et al., 2010; Gillis & Roberts, 1999). Phase relations for the brines hosted in the Platanistasa contact aureole (Troodos ophiolite) constrain trapping pressures to be ~0.1 GPa, that is, lithostatic conditions (Gillis & Roberts, 1999).

The presence of brine at the base of hydrothermal systems, perhaps forming a basal layer (e.g., Bischoff & Rosenbauer, 1989; Lowell & Germanovich, 1997) or being segregated in small fissures and dead ends (Fontaine & Wilcock, 2006), has been hypothesized to explain salinity variations in seafloor hydrothermal vent fluids. Such brines result from phase separation of seawater-derived fluids, with the brine and vapor

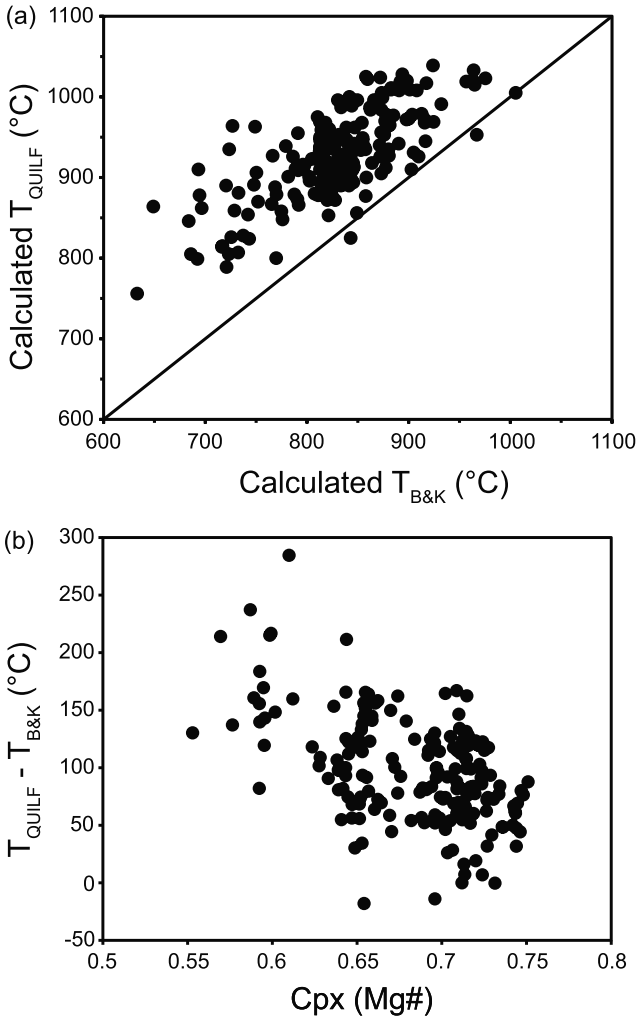

Figure 4. Comparison of different two-pyroxene thermometers: (a) Two pyroxene temperatures for all field areas calculated using the Brey and Köhler (1990; B&K) and Andersen et al. (1993; QUILF) thermometers. The line shows a 1:1 correlation. Temperatures calculated using the QUILF method are systematically higher than those calculated using the Brey and Köhler method; see text for discussion. The average difference between thermometers is 98 ± 47 °C (n = 183). Reported uncertainties for QUILF and Brey and Köhler (1990) are ±30 °C. (b) The difference between the calculated temperatures (ΔT) using QUILF and Brey and Köhler as a function of clinopyroxene Mg#. ΔT is smaller for the more magnesian samples, consistent with the Brey and Köhler thermometer being developed for ultramafic rocks with bulk compositions with Mg# >0.8. Hole 1256D pyroxene data from Alt et al. (2010) were used to calculate temperatures using Andersen et al. (1993). See Figure 6 for data sources for pyroxene compositions from other locations.

being physically separated (at least temporally) by a variety of processes. If a brine layer exists at the base of the hydrothermal system it could have significant implications for the heat transport from the magmatic to hydrothermal systems. However, fluid inclusions hosted in the contact aureoles do not lend support to the existence of a brine layer, as the observed brines are restricted to the volumetrically small felsic igneous lithologies. Dikes from the field areas do host fluid inclusions with higher than seawater salinities (up to 10 wt%, mostly ≤6%), but there are insufficient data to evaluate if there are systematic spatial patterns in salinity (Alt et al., 2010; Gillis, 2002; Heft et al., 2008; Nehlig et al., 1994; Saccocia & Gillis, 1995). Hence, while this is an important problem, the geological record thus far cannot definitively test the hypotheses regarding the role of brine formation.

3. Thermal Constraints

In this section, we first evaluate the various geothermometers that have been applied to determine metamorphic temperatures in CBLs (section 3.1. which can be skipped by nonpetrologists). We then compile an internally consistent set of metamorphic temperatures for the different study areas and show that the average recrystallization temperatures for granulite and hornblende hornfels are 930° ± 59 °C (1σ) and 851° ± 58 °C (1σ) (after correcting for composition, see below), respectively.

3.1. Thermometry Methods

Before presenting an analysis of new and published data, three thermometers that have been used to determine temperatures of recrystallization within the CBL are evaluated: the two-pyroxene thermometers of Andersen et al. (1993; QUILF) and Brey and Köhler (1990) and the amphibole-plagioclase thermometers of Holland and Blundy (1994). Some studies of oceanic hornfels include temperatures derived using the Ernst and Liu (1998) semiquantitative Ti-in-amphibole thermometer (e.g., Alt et al., 2010); because these data are not comparable to quantitative temperatures derived from other thermometers, they are not discussed here. Likewise, the Al-in-clinopyroxene thermometer of France et al. (2010) is not considered because of both the lack of a theoretical basis for this thermometer, and the difference in $a(SiO_2)$ between the natural samples (commonly quartz bearing) and the experiments this is calibrated on (some olivine bearing), which must affect the tschermak component of clinopyroxene. For our analysis of the thermometers we use temperature data for all of the study sites calculated using new and published data or, if the mineral data was not provided in a publication, temperatures were compiled if sufficient information was provided about assumptions made in the calculations.

Temperatures for the granulite hornfels calculated using two-pyroxene (clinopyroxene-orthopyroxene) assemblages are evaluated first. Overall, the metamorphic temperatures derived using the Brey and Köhler thermometer are on average ~100° (±50 °C, 1σ) lower than those derived using the QUILF thermometer (Figure 4a). The Brey and Köhler thermometer was developed for rocks with significantly higher bulk Mg#s ($Mg/Mg + Fe^{2+} > 0.80$) than are typical for hornfels (~0.40 to 0.65). Hence, the impact of bulk composition on calculated temperatures is evaluated using clinopyroxene Mg# as a proxy for bulk composition (Figure 4b). There is a broad negative correlation between the temperature difference between the QUILF and Brey and Köhler thermometers and clinopyroxene Mg# (Figure 4b). These thermometers give similar temperatures where the

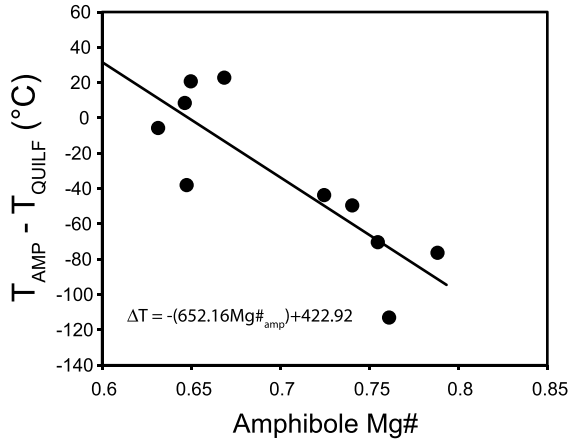

Figure 5. The difference between average equilibration temperatures calculated using QUILF (Andersen et al., 1993) and the amphibole-plagioclase (Holland & Blundy, 1994) thermometer (edenite-tremolite) as a function of amphibole Mg#. Amphibole Mg# ($Mg/(Fe^{2+} + Mg)$) was calculated using the stoichiometry of Holland and Blundy (1994). To produce an internally consistent data set, the correlation of ΔT and Mg# is used to correct all amphibole-plagioclase derived equilibration temperatures to match QUILF temperatures. Temperatures calculated using Holland and Blundy (1994) may be corrected for the compositional dependency of the thermometer: $T_{corrected} = T_{H\&B} + (652.16Mg\#_{amp}) - 423$. Data from Troodos, Oman, and Pito Deep are used to define this relationship; see Figure 6 for data sources. Data from Hole 1256D were not included because individual amphibole compositions are required for this analysis and average compositions are reported (Koepke et al., 2008).

clinopyroxene Mg# is within the range of the Brey and Köhler (1990) calibration but diverge at the lower Mg#s typical of oceanic hornfels. Based on this, we consider the QUILF thermometer to be better suited for studies of oceanic hornfels.

Temperatures derived using the QUILF two-pyroxene thermometer (Andersen et al., 1993) are next compared to temperatures derived from the amphibole-plagioclase thermometer of Holland and Blundy (1994). For this to have meaning, we only use temperatures derived for amphibole interpreted to have formed during peak metamorphic conditions, that is, granular, brown groundmass amphibole that texturally appears to be cogenetic with the two-pyroxene assemblages. Amphibole can form over a wide range of temperature (e.g., Liou et al., 1974); hence, we add a second filter and use an average of the three highest temperatures obtained using the amphibole-plagioclase thermometer to identify the *peak amphibole* temperature. The choice of three is arbitrary and if less than three temperatures are available that meet the peak amphibole criteria we use an average of <3. The hornfels data show that the difference in calculated temperature (ΔT) between the amphibole–plagioclase and QUILF thermometers for a given sample is dependent upon the Mg# ($Mg/Mg + Fe^{2+}$) of the amphibole (Figure 5). This means that calculated temperatures for amphiboles with intermediate Mg#s (≤0.65) are within ±40 °C of the calculated QUILF temperatures (i.e., within uncertainties), whereas for amphibole with higher Mg#s (>0.7), amphibole temperatures may be up to 120 °C lower than QUILF temperatures (Figure 5). This type of compositional dependency for amphibole temperatures was previously noted by Blundy and Cashman (2008), where they document how calculated and experimental temperatures for amphibole diverge as a function of increasing amphibole Mg#. They suggest that this may be due to nonideal interaction between Fe^{2+} and Mg on the M sites that is not accounted for by the amphibole-plagioclase thermometer. Thus, to compare the peak temperatures for amphibole and granulite hornfels, a correction is applied to the amphibole-plagioclase-derived temperatures based on the correlation shown in Figure 5.

In summary, analysis of the three thermometers that have previously been used to study the temperature conditions within the CBL identify problems with their application to the oceanic hornfels collection, making absolute temperatures less well constrained than is optimal. Nevertheless, using an internally consistent approach allows relative temperature differences between samples to be constrained, providing a useful dataset with which to investigate the thermal evolution of the CBL. To this end, we use the QUILF two-pyroxene thermometer, because it is more appropriate for compositions and expected temperatures (~800–1000 °C) of the granulites, alongside the amphibole-plagioclase thermometers of Holland and Blundy (1994) with a correction to a constant amphibole Mg# (0.65) to make these temperatures internally consistent with the two-pyroxene temperatures (Figure 5).

3.2. Peak Temperatures

The recrystallization temperatures recorded by the pyroxene assemblage in the granulite hornfels (Figure 6a) have an average of 930 ± 59 °C (1σ). No significance is attributed to differences between locations because temperatures within contact aureoles vary depending on their proximity to the heat source and country rock temperatures and, with the exception of the Livadia transect (see section 4 and supporting information Text S1 and Figure S2), these positions are not precisely known for the granulite hornfels suites. The amphibole-plagioclase assemblage in the granulite hornfels records slightly lower recrystallization temperatures, with an average of 896 ± 49 °C (using the compositional correction in Figures 5, or 845° ± 62 °C [1σ] without this) because the granulite hornfels recording the highest two-pyroxene temperatures lack amphibole.

The peak temperatures recorded by the hornblende hornfels are shown in Figure 6b. Overall, there is a normal distribution with an average temperature of 851° ± 58 °C (using the compositional correction

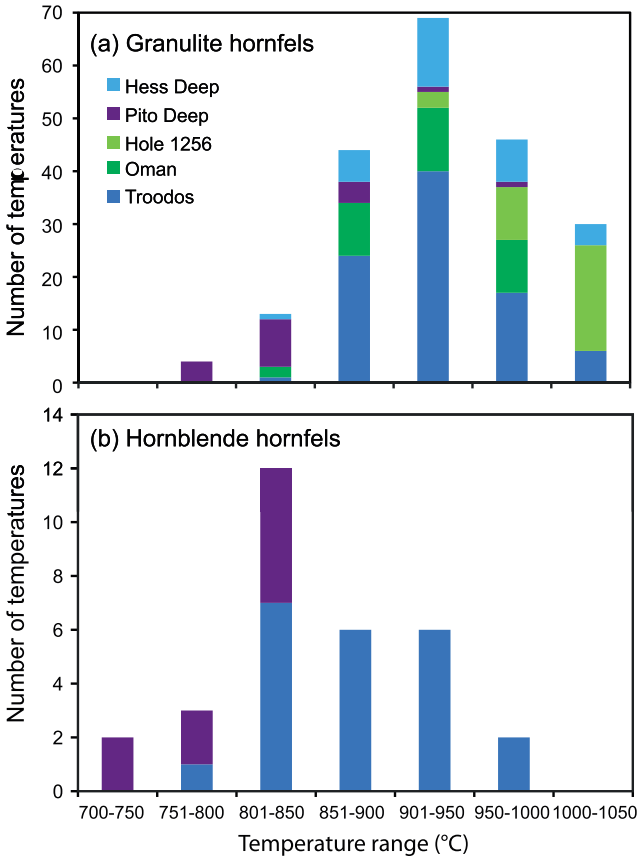

Figure 6. (a) Histogram of equilibration temperatures for two pyroxene assemblages by area. Average of all data: 930 ± 59 °C (1σ). By area: Troodos: 927 ± 42 °C, $n = 88$, $N = 18$ (this study; Gillis & Roberts, 1999; Gillis & Coogan, 2002; Gillis, 2008); Oman: 919 ± 44 °C, $n = 34$, $N = 6$ (Gillis, 2008); Hess Deep: 937 ± 19 °C, $n = 32$, $N = 4$ (this study; Gillis, 2008); Pito Deep: 834 ± 52 °C, $n = 19$, $N = 3$ (this study; Gillis, 2008); Hole 1256D: 1001 ± 28 °C, $n = 33$, $N = 19$ (Alt et al., 2010; France et al., 2009; Koepke et al., 2008; average ± 1σ; n = number of analyses, N = number of samples; new data: supporting information Data Set S1). Data from Koepke and Goetze (2015) were not included as their samples were largely cobbles recovered from external junk baskets and only sample averages were provided. The reported uncertainty for the QUILF (Andersen et al., 1993) thermometer is ±40 °C. (b) Histogram of peak amphibole-plagioclase equilibration temperatures for hornblende hornfels by area. Average of all data: 851 ± 58 °C (using the compositional correction in Figures 5, or 807 ± 46 °C [1σ] without this). By area: Troodos: 874 ± 47 °C, $n = 22$, $N = 9$ (this study; Gillis & Roberts, 1999; Gillis & Coogan, 2002); Pito Deep: 795 ± 40 °C, $n = 9$, $N = 2$ (this study, Gillis, 2008; new data: supporting information Data Set S2). See text for criteria for identifying peak temperature. The reported uncertainty for the Holland and Blundy (1994) thermometer is ±40 °C.

from Figures 5, or 807° ± 46 °C [1σ] without this). The lower temperatures in the hornblende than granulite hornfels is, of course, expected given the difference in mineralogy and that the hornblende hornfels form further from the igneous intrusive contact, that is, the heat source.

Both granulite and hornblende hornfels contain retrograde amphibole, interpreted to have formed after peak metamorphism when brittle deformation allowed fluid ingress into the contact aureole as the system cooled. Calculated temperatures for these amphiboles extend from the lower range of hornblende hornfels (~800 °C; Figure 6) to the lower limit of the thermometer (400 °C; e.g., Alt et al., 2010; Gillis & Roberts, 1999). This reflects the broad temperature stability field for amphibole in hydrous metabasites (e.g., Liou et al., 1974).

4. Temperature Gradients and Heat Fluxes Across the CBL

A well-exposed section of the Platanistasa contact aureole (Troodos ophiolite) was sampled in detail in the Livadia area as part of this study (supporting information Figure S2). Thermometric data for the Livadia transect allows us to examine the paleotemperature profile across a paleo-CBL. Average peak temperatures recorded in the granulite hornfels at Livadia (907 ± 27 °C) overlap the average peak temperatures in the broader Platanistasa region (957 ± 40 °C; Gillis & Roberts, 1999), confirming the representativeness of this area. The peak temperatures along the Livadia transect decrease systematically with height above the underlying gabbros (Figure 7). Taken at face value these data suggest a paleothermal gradient (dT/dz) of 4.2 ± 0.5 °C/m. A similar thermal gradient (3 °C/m) has been proposed for Hole 1256D (Koepke et al., 2008), although it is far less well constrained due to the low recovery of this unit and uncertainty about whether some hornfels in this core are xenoliths rather than part of the CBL (France et al., 2009). Moreover, while this study reported temperatures constrained using four different thermometers, the specific thermometer or combinations of thermometers used to calculate the thermal gradient is not provided, meaning it is not possible to assess uncertainties. Hence, we focus here on the well constrained Livadia paleothermal gradient. Taking the Livadia data at face value, we can calculate the heat flux (Q) across the CBL at Livadia using Fourier's law, such that $Q = -K\,(dT/dz)$, where K is the thermal conductivity (2 W m^{-1} K^{-1}) and dT/dz is the thermal gradient in the CBL. Using the calculated thermal gradients from the Livadia contact aureole, the heat flux was 7.6 to 9.4 W/m^2 or 7.6 to 9.4 MW/km along axis assuming a 1-km-wide AML.

Before comparing the heat flux predicted by the measured thermal gradient in Livadia with other heat flux estimates, it is important to consider what this gradient in metamorphic temperature means. The temperature gradient determined from the raw data implicitly assumes the rocks reached their peak temperature at the same time. This is likely to be a reasonable assumption only for samples from the base of the system, closest to the heat source. Samples further from the heat source may well increase in temperature as the system dies because this will be associated with thickening of the CBL. To illustrate this point, we consider the thermal evolution of the rocks that make up a CBL beneath a vigorous blacksmoker system assuming the magmatic and hydrothermal systems instantaneously shut down. Seafloor heat flow studies suggest that when active, such a system has a heat flux across the CBL of the order of ~100 W/m^2 (e.g., Lowell et al., 2013), requiring a ~12-m thick

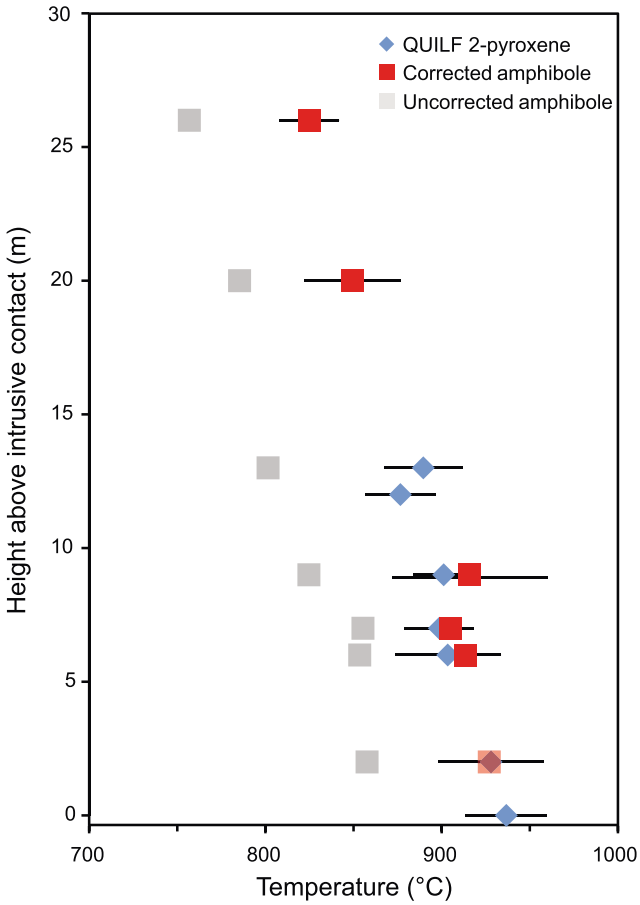

Figure 7. Peak metamorphic temperature versus height above the intrusive contact along the Livadia transect, located within the Platanistasa regional contact aureole. Amphibole-plagioclase temperatures were corrected for the compositional dependency of the Holland and Blundy (1994) thermometer using the relationship shown in Figure 5 to make them internally consistent with the QUILF thermometry; uncorrected amphibole temperatures are shown in gray for comparison. Error bars show the standard deviation (1σ) for all data for the two-pyroxene thermometer and standard deviation (1σ) of the highest ≤3 temperatures for the amphibole-plagioclase thermometer (see text for details).

CBL assuming a magma temperature of 1100 °C, a hydrothermal temperature of 500 °C, and a thermal conductivity of 2 W m^{-1} K^{-1}. If such a system shuts down instantaneously, and heat transport is solely by conduction, the rocks that make up the lower half (6 m) of the CBL during the active stage would cool and hence the peak metamorphic temperature recorded in the rocks would be the temperature when the rocks were part of an active, high heat flux CBL. In contrast, rocks in the upper half of the relic CBL would initially heat up as heat was conducted upward into them—hence the peak metamorphic temperatures recorded in these rocks (~800–850 °C) would be higher than the temperature the rocks were at when they were part of an active highheat flux CBL (~500 °C). This means the temperature gradient recorded by the peak metamorphic temperatures would be less than that when the system was powering a vigorous hydrothermal system. Of course, this end-member scenario is not realistic, and the exact thermal evolution of a CBL as the system wanes will differ depending on numerous factors. However, it illustrates the concept that thermal relaxation as the power output across the CBL wanes will lead to the peak temperatures in the rock record underestimating the temperature gradient and hence peak heat flux.

We now compare the heat flux calculated for the Livadia contact aureole to theoretical predictions for the steady state heat flux that results from magmatic construction (e.g., Cannat et al., 2004; Wilcock & Delaney, 1996):

$$Q = hs\rho(L + c(T_l - T_s))$$

where h is the thickness of the lower crust (3,000–4,000 m), s is spreading rate (1.6 to 4.7 × 10^{-9} m/s; 5–15 cm/year), ρ is density of basalt (2,800 kg/m^3), L is the latent heat of crystallization (420–500 kJ/kg), c is the specific heat capacity of the lower crust (1,400–1,600 J kg^{-1} C^{-1}), and T_l (1250–1200 °C) and T_s (1040 °C) are liquidus and solidus temperatures, respectively (input from: Cannat et al., 2004; Liu & Lowell, 2009). We assume that the lower crust is not entirely solidified on axis (solid fraction ~0.9 to 0.95) and that the heat of lower crustal accretion is lost through the roof of the AML, thus providing an upper limit of the heat flux through the CBL. This yields a steady state heat flux out of the AML of 8 to 26 MW/km, assuming an AML width of 1 km (equivalent to a temperature gradient of 4–13 °C/m; Figure 8). The minimum heat flux recorded in the Livadia paleo-CBL falls within this range, but at the lower end, consistent with the suggestion that fossil temperature gradients are minima. Heat extraction from a larger area would also lead to a lower thermal gradient in the CBL, but seismic data do not suggest the AML roof is much wider than 1 km.

The heat fluxes calculated for the Livadia paleo-CBL, and those predicted for steady state crustal accretion, are about an order of magnitude smaller than estimates of the heat output from hydrothermal vent fields (Figure 8). For example, heat flux values for active vent fields along the northern EPR and Juan de Fuca ridge range from 100–500 MW/km (see summary in Lowell et al., 2013). While there are significant uncertainties associated with comparing these kinds of disparate data, these differences in heat flux appear to be too large to be simply due to uncertainties in the methodologies. Instead, the much higher heat fluxes for the active vent sites suggest they are associated with ephemeral conditions when the CBL is thin, with very steep thermal gradients (50–250 °C/m), likely associated with magmatic replenishment, rather than reflective of steady state conditions (e.g., Liu & Lowell, 2009; Lowell et al., 2013; Wilcock et al., 2009). Indeed, these estimates come from study areas selected specifically for having abundant high temperature seafloor hydrothermal activity.

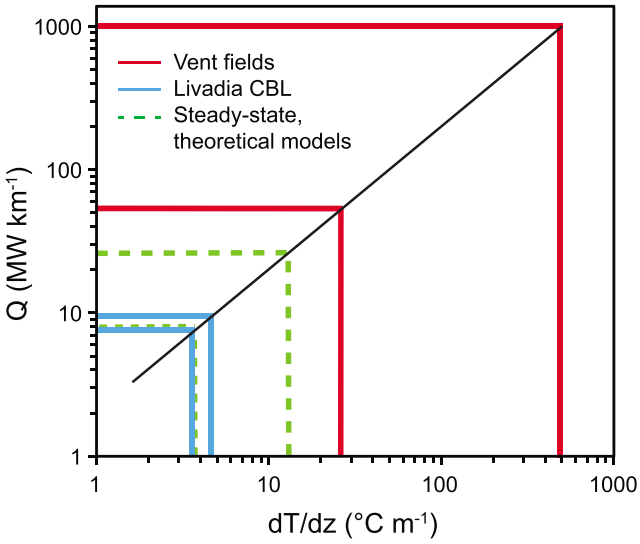

Figure 8. Heat fluxes and associated thermal gradients (d*T*/d*z*) in the conductive boundary layer (CBL) for active vent fields at intermediate- to fast-spreading ridges (Lowell et al., 2013, includes twofold uncertainty), theoretical steady state segment models (see text), and the Livadia paleo-CBL (which is a minimum value; see text). Solid and dashed lines bracket the range in values. All heat fluxes assume a 1-km-wide axial magma lens.

5. Evolution of the CBL

The geological constraints on the CBL reviewed in the previous sections are discussed here from bottom-to-top in the context of seismic, heat flow, and vent fluid observations from modern systems. The data all point to CBLs being dynamic with rapidly changing thermal and rheological conditions. Active blacksmoker systems are powered only by one end-member style of CBL (thin with a steep thermal gradient), but these conditions are transient and are not the normal state of ridge segments (Figure 9).

5.1. The Base of the CBL: Thinning From below

The existence of a magma body at the base of the CBL along intermediate- to fast-spreading ridges leads to high-temperature prograde metamorphism of the base of the overlying sheeted dikes as evidenced by the contact aureoles described above. The granulite hornfels found in the lower half of the aureoles provide evidence for very high temperatures at the base of CBLs (~930 °C) and lithostatic pressures (~0.1 GPa). At these conditions the rocks are ductile, as evidenced by the swirly dike margins (Figure 2c), and as expected based on experiments conducted under these *P-T* conditions and extrapolated to natural strain rates for tectonic spreading (e.g., Hirth et al., 1998; Violay et al., 2012; Violay et al., 2015). This leads to a nearly impermeable base to the CBL.

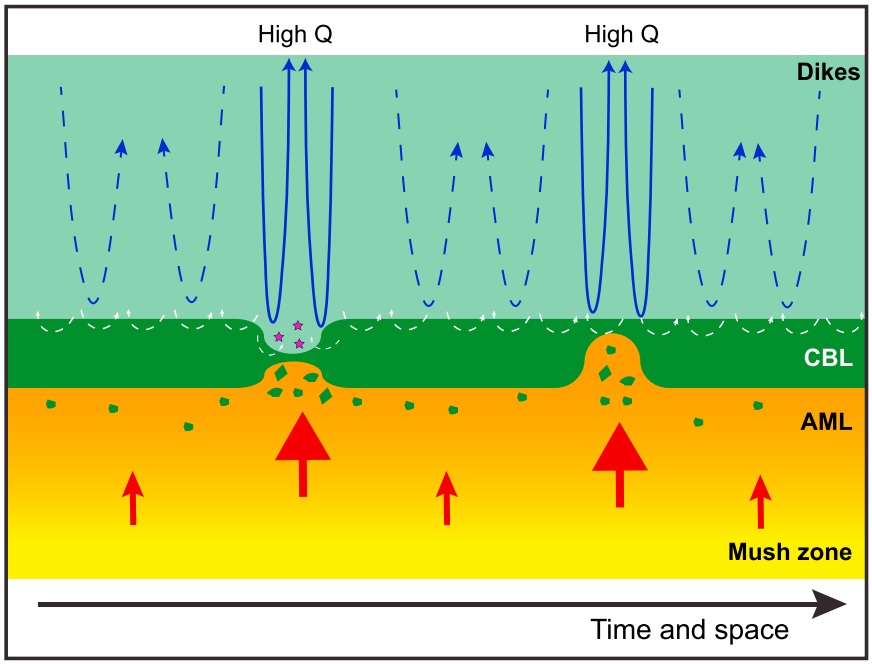

Figure 9. Schematic illustration of the magma-hydrothermal transition showing how the thickness and character of the conductive boundary layer (CBL) change in time and space (horizontal axis) in response to changing magma supply rates (red arrows). The CBL is thick when the magma supply is relatively slow (red small arrows), leading to low seafloor heat fluxes, reflecting less vigorous hydrothermal flow (blue dashed lines). The CBL thins from below as the axial magma lens (AML) shallows in response to periods of enhanced magma supply (red large arrow); the base of the CBL partial melts and disaggregates, leading to xenoliths being stoped into the AML. The CBL may also thin from above by ephemeral cracking (red stars) due, for example, to magma sill inflation or thermal stresses. CBL thinning temporally increases the seafloor heat output, invigorating hydrothermal fluid flow (blue solid lines) and creating or reinvigorating high temperature hydrothermal vent sites. There is limited exchange of fluids across the top of the CBL and the dike-hosted hydrothermal system (white dashed arrows). The relative fraction of thin versus thick CBLs in time and space is not well constrained, however, thicker CBLs are expected to be the more common state. Vertical axis is not to scale.

The common occurrence of xenoliths in the uppermost plutonics (Figure 2f), and the overenrichment of Cl in lavas (section 2.2) provides strong evidence that the CBL is thinned from below by stoping blocks off its base and assimilating them into the AML. This process is probably aided by partial melting of the CBL as evidenced by felsic bodies within the lower part of the CBL (section 2.3.3). Partial melting acts as a (local) heat sink (the latent heat of fusion) and must weaken the rocks, facilitating disaggregation of the base of the CBL and hence stoping. Melt fractions of ~30%–40% are sufficient to make rocks behave more like a liquid than a solid (e.g., Rushmer, 1996; Vigneresse et al., 1996) and even lower melt fractions can dramatically weaken rocks (e.g., Rosenberg & Handy, 2005). Thus, as the rocks partially melt, it is likely that they will disaggregate and blocks will be entrained into the underlying magma with their position being taken by magma—that is, the roof of the AML will move upward thinning the CBL (Figure 9). The partial melting and disaggregation of the CBL relies on the magmatic heat flux being sufficient to sustain this process, which will generally require frequent replenishment (e.g., Liu & Lowell, 2009; Wilcock et al., 2009). During times when the magmatic heat flux is sufficient for disaggregation of the base of the CBL to occur, this process will efficiently keep the CBL thin leading to high heat fluxes across the CBL into the overlying hydrothermal system. In this model the peak temperatures recorded by rocks in the base of paleo-CBLs reflect the maximum temperature the CBL can reach before it is broken apart. This mechanism of CBL thinning will be aseismic and can only be sustained while magma supply rates are higher than those required for steady state crustal accretion and thus during short-lived episodes.

Despite the very high temperatures recorded by rocks from the base of paleo-CBLs (Figures 6 and 7), and evidence they behave in a ductile manner under some conditions (Figure 2c), the occurrence of felsic veins indicates that they can also behave in a brittle manner. Additionally, the base of the CBL must fracture for dikes to be emplaced. High strain rates, for example, due to magma replenishment or magmatic volatile exsolution can fracture the base of the CBL. Such fracturing events will allow direct transfer of mass from the AML into the hydrothermal system (e.g., magmatic volatiles and metal species carried with them). Evidence for direct transfer of magmatic volatiles into the hydrothermal system comes both from observations of vent fluid being enriched in magmatic components (e.g., CO_2 and He) following subsurface magmatic events (Lilley et al., 2003; Seyfried et al., 2003; Von Damm & Lilley, 2004) and the composition of minerals in the uppermost plutonics (Section 2.4).

5.2. Variable Temperature Gradients Across the CBL

The temperature gradient across the CBL controls the heat flux from the magmatic system into hydrothermal fluids. Data from numerous sources provide compelling evidence that the CBL thickness is spatially and temporally variable leading to temporal and spatial variability in hydrothermal fluxes. At one end-member, estimates of the heat fluxes out of vent fields suggest heat fluxes of roughly 100–500 MW/km along axis (Lowell et al., 2013), which requires temperature gradients in the CBL of 50–250 °C/m (Figure 8). Such steep thermal gradients, and hence thin boundary layers (~2 to 10 m; Lowell & Germanovich, 2004), would be inherently unstable, and these high heat fluxes could only be maintained by continually disaggregating the base of the CBL through partial melting and stoping. In turn, frequent replenishment is required to fuel this process (e.g., Liu & Lowell, 2009). Because such high heat fluxes are substantially greater than the steady state heat flux (Figure 8), black smokers with such high power output can only be present for a small fraction of the life cycle of a crustal section. Evidence that thicker CBLs, and hence lower heat fluxes into the hydrothermal system, are more the common state of ridge segments comes from several lines of evidence. First, simple thermal balance arguments (section 4) suggest that steady state temperature gradients in the CBL are $<$20 °C/m and generally substantially less than this (i.e., a CBL $>$30-m thick for a 600 °C temperature drop; Figure 8). Since some fraction of heat is lost during times when the CBL is thin, and high power output black smoker systems are operating, the CBL must be even thicker than this at other times (Figure 9). Second, lower thermal gradients during typical conditions are also consistent with observations from the Livadia contact aureole (Figure 7). Finally, large variations in the thickness of the high seismic velocity region immediately above the AML (up to ~200 m), and variations in how close to the roof of the AML microseismicity occurs, are both consistent with variations in the thickness of the CBL (Arnoux et al., 2017; Marjanovic et al., 2017; Singh et al., 1999; Weekly et al., 2014). Overall, the data suggest that systems evolve from thin CBLs when replenishment is frequent to thicker CBLs when replenishment is less frequent (Figure 9).

Black smoker systems, where estimates of ridge axis hydrothermal power outputs come from, are generally found by identifying regions with water column signatures of hydrothermal activity and zooming in on these (e.g., Baker et al., 2016). Hence, it should be expected that the hydrothermal heat flux from these regions is greater than the steady state heat flux. This suggests that active hydrothermal systems are not representative of the common state of ridge segments. If correct, this raises a question of how representative global estimates of properties such as chemical fluxes from hydrothermal vents are, when the vast majority of such data comes from these transient systems. Whether *normal* hydrothermal conditions, with thicker CBLs and smaller hydrothermal heat fluxes, lead to substantially different element/heat fluxes needs careful consideration.

5.3. The Top of the CBL

The geological relationships at the top of the CBL, with the outcrops becoming progressively more fractured and the rocks gradually less recrystallized upward, suggest that this is a gradational boundary. Amphibole veins within the CBL indicate it can fracture and seawater-derived fluids penetrate down into it from above at temperatures ≥700 °C (Gillis & Roberts, 1999). Further evidence of fracturing in the CBL comes from microseismicity, which appears to extend into some high seismic velocity regions above AMLs that are interpreted to be a CBL (Tolstoy et al., 2008; Waldhauser & Tolstoy, 2011; Wilcock et al., 2009). The driving mechanisms for fracturing could be internal to the CBL, for example, related to increases in pore fluid pressures due to devolatilization reactions and/or hydrous partial melting (e.g., Dutrow & Norton, 1995; Hanson, 1995). Additionally, thermal stresses within the dikes (e.g., Sohn et al., 1999), or related to magma sill inflation events (Wilcock et al., 2009), could lead to fracturing of the CBL from above. The fluids that penetrate into the CBL from above when it cracks would probably transport a negligible amount of heat back into the overlying hydrothermal cell (Figure 9). However, it is less clear whether these fluids would have sufficiently different compositions to fluids that react at ~400 °C (i.e., dike-hosted fluids) so as to be an important mixing end-member in the overlying hydrothermal fluids.

A number of studies have suggested that the CBL thickens upward into the dikes through precipitation of hydrothermal minerals filling pore space (e.g., Arnoux et al., 2017; Wilcock & Delaney, 1996). Although the relationships between seismic velocity, porosity, and permeability are complex (e.g., Carlson, 2014), the variation in Vp in the roof zone of the AML along the Juan de Fuca ridge of ~1 km/s would seem to be too large to be explained simply by mineral precipitation. There is no evidence in the lower dikes of the ophiolites discussed here for large amounts of pore space being filled with secondary phases and so unless anhydrite precipitation, and subsequent dissolution, is called on it seems unlikely that clogging of pore space by secondary mineral precipitation has a large effect on permeability or seismic velocity. Alternative explanations for higher velocities in some areas above the AML include that these could be relic CBLs, composed of hornfelsic rocks with low permeabilities, or they could be plutonic rocks plated to the roof of the AML during times of waning magma supply. Indeed, these regions could be the geological record of fluctuations in the depth of AMLs along ridge segments on short length scales that have been documented along intermediate- to fast-spreading ridges.

Acknowledgments
We thank M. Raudsepp and E. Czech for their assistance in the probe lab and Petrus le Roux and two anonymous reviewers for their comments. All data are provided in supporting information, or in the cited references or associated supplementary material associated with these. K. M. G. and L. A. C. were funded through NSERC Discovery (5098 and 155396) and Accelerator grants. The manuscript was prepared while the authors were guests at the Institute of Marine Sciences in Barcelona.

References

Alt, J. C., Laverne, C., Coggon, R. M., Teagle, D. A. H., Banerjee, N. R., Morgan, S., et al. (2010). Subsurface structure of a submarine hydrothermal system in ocean crust formed at the East Pacific Rise, ODP/IODP Site 1256. *Geochemistry, Geophysics, Geosystems*, *11*, Q10010. https://doi.org/10.1029/2010GC003144

Andersen, D. L., Lindsley, D. H., & Davidson, P. M. (1993). Quilf: A Pascal program to assess equilibria among Fe-mg-Mn-Ti oxides, pyroxenes, olivine and quartz. *Computers and Geosciences*, *19*(9), 1333–1350. https://doi.org/10.1016/0098-3004(93)90033-2

Arnoux, G. M., Toomey, D. R., Hooft, E. E. E., Wilcock, W. S. D., Morgan, J., Warner, M., & VanderBeek, B. P. (2017). Seismic evidence that black smoker heat flux is influenced by localized magma replenishment and associated increases in crustal permeability. *Geophysical Research Letters*, *44*, 1687–1695. https://doi.org/10.1002/2016GL071990

Baker, E. T., Resing, J. A., Haymon, R. M., Tunnicliffe, V., Lavelle, J. W., Martinez, F., et al. (2016). How many vent fields? New estimates of vent field populations on ocean ridges from precise mapping of hydrothermal discharge locations. *Earth and Planetary Science Letters*, *449*, 186–196. https://doi.org/10.1016/j.epsl.2016.05.031

Beard, J. S., & Lofgren, G. E. (1991). Dehydration melting and water-saturated melting of basaltic and andesitic greenstones and amphibolites. *Journal of Petrology*, *32*(2), 365–401. https://doi.org/10.1093/petrology/32.2.365

Bischoff, J. L., & Rosenbauer, R. J. (1989). Salinity variations in submarine hydrothermal systems by layered double-diffusive convection. *Journal of Geology*, *97*(5), 613–623. https://doi.org/10.1086/629338

Blundy, J., & Cashman, K. (2008). Petrologic reconstruction of magmatic system variables and processes. In K. D. Putirka & F. J. Tepley (Eds.), *Minerals, inclusions and volcanic processes* (Vol. 69, pp. 179–239). Chantilly: Mineral. Soc. Amer.

Brey, G. P., & Köhler, T. (1990). Geothermobarometry in four-phase lherzolites II. New thermobarometers, and practical assessment of existing thermobarometers. *Journal of Petrology*, *31*(6), 1353–1378. https://doi.org/10.1093/petrology/31.6.1353

Cann, J. R., Strens, M. R., & Rice, A. (1985). A simple magma-driven thermal balance model for the formation of volcanogenic massive sulphides. *Earth and Planetary Science Letters*, *76*(1-2), 123–134. https://doi.org/10.1016/0012-821X(85)90153-0

Cannat, M., Cann, J., & Maclennan, J. (2004). Some hard rock constraints on the supply of heat to mid-ocean ridges. In C. R. German, J. Lin, & L. M. Parson (Eds.), *Mid-ocean ridges: hydrothermal interactions between the lithosphere and oceans* (Vol. 148, pp. 111–149). Washington, DC: American Geophysical Union.

Carlson, R. L. (2014). The influence of porosity and crack morphology on seismic velocity and permeability in the upper oceanic crust. *Geochemistry, Geophysics, Geosystems*, *15*, 10–27. https://doi.org/10.1002/2013GC004965

Coogan, L. A., Wilson, R. N., Gillis, K. M., & MacLeod, C. J. (2001). Near-solidus evolution of oceanic gabbros: Insights from amphibole geochemistry. *Geochimica et Cosmochimica Acta*, *65*(23), 4339–4357. https://doi.org/10.1016/S0016-7037(01)00714-1

Dutrow, B., & Norton, D. (1995). Evolution of fluid pressure and fracture propagation during contact metamorphism. *Journal of Metamorphic Geology*, *13*(6), 677–686. https://doi.org/10.1111/j.1525-1314.1995.tb00251.x

Erdmann, M., Fischer, L. A., France, L., Zhang, C., Godard, M., & Koepke, J. (2015). Anatexis at the roof of an oceanic magma chamber at IODP Site 1256 (equatorial Pacific): An experimental study. *Contributions to Mineralogy and Petrology*, *169*(4), 39. https://doi.org/10.1007/s00410-015-1136-5

Ernst, W. G., & Liu, J. (1998). Experimental phase-equilibrium study of Al- and Ti-contents of calcic amphibole in MORB—A semiquantitative thermobarometer. *American Mineralogist*, *83*(9–10), 952–969. https://doi.org/10.2138/am-1998-9-1004

Fontaine, F. F., & Wilcock, W. S. D. (2006). Dynamics and storage of brine in mid-ocean ridge hydrothermal systems. *Journal of Geophysical Research*, *111*, B06102. https://doi.org/10.1029/2005JB003866

Fontaine, F. J., Olive, J. A., Cannat, M., Escartin, J., & Perol, T. (2011). Hydrothermally-induced melt lens cooling and segmentation along the axis of fast- and intermediate-spreading centers. *Geophysical Research Letters*, *38*, L14307. https://doi.org/10.1029/2011GL047798

France, L., Ildefonse, B., & Koepke, J. (2009). Interactions between magma and hydrothermal system in Oman ophiolite and in IODP hole 1256D: Fossilization of a dynamic melt lens at fast spreading ridges. *Geochemistry, Geophysics, Geosystems*, *10*, Q10O19. https://doi.org/10.1029/2009GC002652

France, L., Ildefonse, B., & Koepke, J. (2013). Hydrous magmatism triggered by assimilation of hydrothermally altered rocks in fossil oceanic crust (northern Oman ophiolite). *Geochemistry, Geophysics, Geosystems*, *14*, 2598–2614. https://doi.org/10.1002/ggge.20137

France, L., Koepke, J., Ildefonse, B., Cichy, S. B., & Deschamps, F. (2010). Hydrous partial melting in the sheeted dike complex at fast spreading ridges: Experimental and natural observations. *Contributions to Mineralogy and Petrology*, *160*(5), 683–704. https://doi.org/10.1007/s00410-010-0502-6

France, L., Koepke, J., MacLeod, C. J., Ildefonse, B., Godard, M., & Deloule, E. (2014). Contamination of MORB by anatexis of magma chamber roof rocks: Constraints from a geochemical study of experimental melts and associated residues. *Lithos*, *202*, 120–137.

Gillis, K. M. (2002). The rootzone of an ancient hydrothermal system exposed in the Troodos ophiolite, Cyprus. *Journal of Geology*, *110*(1), 57–74. https://doi.org/10.1086/324205

Gillis, K. M. (2008). The roof of an axial magma chamber: A hornfelsic heat exchanger. *Geology*, *36*(4), 299–302. https://doi.org/10.1130/G24590A.1

Gillis, K. M., & Coogan, L. A. (2002). Anatectic migmatites from the roof of an ocean ridge magma chamber. *Journal of Petrology*, *43*(11), 2075–2095. https://doi.org/10.1093/petrology/43.11.2075

Gillis, K. M., Coogan, L. A., & Chaussidon, M. (2003). Volatile behavior (Cl, F, B) in the roof of an axial magma chamber from the East Pacific Rise. *Earth and Planetary Science Letters*, *213*(3-4), 447–462. https://doi.org/10.1016/S0012-821X(03)00346-7

Gillis, K. M., Muehlenbachs, K., Stewart, M., Karson, J., & Gleeson, T. (2001). Fluid flow patterns in fast-spreading East Pacific Rise crust exposed at Hess Deep. *Journal of Geophysical Research*, *106*(B11), 26311–26329. https://doi.org/10.1029/2000JB000038

Gillis, K. M., & Roberts, M. (1999). Cracking at the magma-hydrothermal transition: Evidence from the Troodos ophiolite. *Earth and Planetary Science Letters*, *169*(3-4), 227–244. https://doi.org/10.1016/S0012-821X(99)00087-4

Gregory, R. T., & Taylor, H. P. (1981). An oxygen isotope profile in a section of Cretaceous oceanic crust, Samail ophiolite, Oman: Evidence for $\delta^{18}O$ buffering of the oceans by deep (>5km) seawater-hydrothermal circulation at mid-ocean ridges. *Journal of Geophysical Research*, *86*(B4), 2737–2755. https://doi.org/10.1029/JB086iB04p02737

Hanson, R. B. (1995). The hydrodynamics of contact metamorphism. *Geological Society of America Bulletin*, *107*(5), 595–611. https://doi.org/10.1130/0016-7606(1995)107<0595:THOCM>2.3.CO;2

Heft, K. L., Gillis, K. M., Pollock, M. A., Karson, J. A., & Klein, E. M. (2008). Role of upwelling hydrothermal fluids in the development of alteration patterns at fast spreading ridges: Evidence from the sheeted dike complex at Pito Deep. *Geochemistry, Geophysics, Geosystems*, *9*, Q05O07. https://doi.org/10.1029/2007GC001926

Hirth, G., Escartin, J., & Lin, J. (1998). The rheology of the lower oceanic crust: Implications for lithospheric deformation at mid-ocean ridges. In W. R. Buck, P. T. Delaney, J. A. Karson, & Y. Lagabrielle (Eds.), *Faulting and magmatism at mid-ocean ridges* (Vol. 106, pp. 291–303). Washington, DC: American Geological Union.

Holland, T., & Blundy, J. (1994). Non-ideal interactions in calcic amphiboles and their bearing on amphibole-plagioclase thermometry. *Contributions to Mineralogy and Petrology*, *116*(4), 433–447. https://doi.org/10.1007/BF00310910

Juteau, T., Manac'h, G., Moreau, O., Lecuyer, C., & Ramboz, C. (2000). The high temperature reaction zone of the Oman ophiolite: New field data, microthermometry of fluid inclusions, PIXE analyses and oxygen isotopic ratios. *Marine Geophysical Researches*, *21*(3/4), 351–385. https://doi.org/10.1023/A:1026798811446

Karson, J. A. (2002). Geologic structure of the uppermost oceanic crust created at fast- to intermediate-rate spreading centers. *Annual Review of Earth and Planetary Sciences*, *30*, 13.11–13.38.

Kelley, D. S., & Malpas, J. (1996). Melt-fluid evolution in gabbroic rocks from Hess Deep. In C. Mével, K. M. Gillis, J. Allen, & P. Meyer (Eds.), *Proc. ODP, Sci. Results* (Vol. 147, pp. 213–226). College Station, TX: Ocean Drilling Program.

Kelley, D. S., Robinson, P. T., & Malpas, J. G. (1992). Processes of brine generation and circulation in the oceanic crust: Fluid inclusion evidence from the Troodos Ophiolite, Cyprus. *Journal of Geophysical Research*, *97*(B6), 9307–9322. https://doi.org/10.1029/92JB00520

Kirchner, T. M., & Gillis, K. M. (2012). Mineralogical and strontium isotopic record of hydrothermal processes in the lower ocean crust at and near the East Pacific Rise. *Contributions to Mineralogy and Petrology*, *164*(1), 123–141. https://doi.org/10.1007/s00410-012-0729-5

Koepke, J., Christie, D. M., Dziony, W., Holtz, F., Lattard, D., Laclennan, J., et al. (2008). Petrography of the dikegabbro transition at IODP site 1256 (equatorial Pacific): The evolution of the granoblastic dikes. *Geochemistry, Geophysics, Geosystems*, *9*, Q07O09. https://doi.org/10.1029/2008GC001939

Koepke, J., & Goetze, N. (2015). Data report: Microanalytical and geothermometric investigations on granoblastic dikes from the gabbro–dike transition from Hole 1256D (IODP Expedition 335, East Pacific Rise). In D. A. H. Teagle, B. Ildefonse, P. Blum, & E. Scientists (Eds.),

Proc. IODP (Vol. 335). Tokyo: Integrated Ocean Drilling Program Management International. https://doi.org/10.2204/iodp.proc.335.201.2015

le Roux, P. J., Shirey, S. B., Hauri, E. H., Perfit, M. R., & Bender, J. F. (2006). The effects of variable sources, processes and contaminants on the composition of northern EPR MORB (8-10 degrees N and 12-14 degrees N): Evidence from volatiles (H_2O, CO_2, S) and halogens (F, cl). *Earth and Planetary Science Letters*, *251*(3–4), 209–231.

Lilley, M. D., Butterfield, D. A., Lupton, J. E., & Olson, E. J. (2003). Magmatic events can produce rapid changes in hydrothermal vent chemistry. *Nature*, *422*(6934), 878–881. https://doi.org/10.1038/nature01569

Liou, J. G., Kuniyoshi, S., & Ito, K. (1974). Experimental studies of the phase relations between greenschist and amphibolite in a basaltic system. *American Journal of Science*, *274*(6), 613–632. https://doi.org/10.2475/ajs.274.6.613

Lister, C. R. B. (1974). On the penetration of water into hot rock. *Geophysical Journal of the Royal Astronomical Society*, *39*(3), 465–509. https://doi.org/10.1111/j.1365-246X.1974.tb05468.x

Lister, C. R. B. (1983). On the intermittency and crystallization mechanisms of sub-seafloor magma chambers. *Geophysical Journal of the Royal Astronomical Society*, *73*(2), 351–365. https://doi.org/10.1111/j.1365-246X.1983.tb03320.x

Liu, L., & Lowell, R. P. (2009). Models of hydrothermal heat output from a convecting, crystallizing, replenished magma chamber beneath an oceanic spreading center. *Journal of Geophysical Research*, *114*, B02102. https://doi.org/10.1029/2008JB005846

Lowell, R. P., & Burnell, D. K. (1991). Mathematical modeling of conductive heat transfer from a freezing, convecting magma chamber to a single-pass hydrothermal system: Implications for seafloor black smokers. *Earth and Planetary Science Letters*, *104*(1), 59–69. https://doi.org/10.1016/0012-821X(91)90237-C

Lowell, R. P., Farough, A., Hoover, J., & Cummings, K. (2013). Characteristics of magma-driven hydrothermal systems at oceanic spreading centers. *Geochemistry, Geophysics, Geosystems*, *14*, 1756–1770. https://doi.org/10.1002/ggge.20109

Lowell, R. P., & Germanovich, L. N. (1994). On the temporal evolution of high-temperature hydrothermal systems at ocean ridge crests. *Journal of Geophysical Research*, *99*(B1), 565–575. https://doi.org/10.1029/93JB02568

Lowell, R. P., & Germanovich, L. N. (1997). Evolution of a brine-saturated layer at the base of a ridge-crest hydrothermal system. *Journal of Geophysical Research*, *102*(B5), 10,245–10,255. https://doi.org/10.1029/97JB00264

Lowell, R. P., & Germanovich, L. N. (2004). Hydrothermal processes at mid-ocean ridges: Results from scale analysis and single-pass models. In C. R. German, J. Lin, & L. M. Parson (Eds.), *Mid-ocean ridges: hydrothermal interactions between the lithosphere and oceans* (Vol. 148, pp. 219–244). Washington, DC: American Geophysical Union.

Malpas, J. (1990). Crustal accretionary processes in the Troodos ophiolite, Cyprus: evidence from field mapping and deep crustal drilling. In J. Malpas, E. M. Moores, A. Panayiotou, & C. Xenophontos (Eds.), *Ophiolites: Oceanic Crustal Analogues* (pp. 65–74). Nicosia: Cyprus Geological Survey Department.

Manning, C. E., & Bird, D. K. (1986). Hydrothermal clinopyroxenes of the Skaergaard intrusion. *Contributions to Mineralogy and Petrology*, *92*(4), 437–447. https://doi.org/10.1007/BF00374426

Marjanovic, M., Fuji, N., Singh, S. C., Belahi, T., & Escartin, J. (2017). Seismic signatures of hydrothermal pathways along the East Pacific Rise between 9 degrees 16 ' and 9 degrees 56 ' N. *Journal of Geophysical Research: Solid Earth*, *122*, 10,241–10,262. https://doi.org/10.1002/2017JB015004

Michael, P. J., & Cornell, W. C. (1998). Influence of spreading rate and magma supply on crystallisation and assimilation beneath mid-ocean ridges: Evidence from chlorine and major element chemistry of mid-ocean ridge basalts. *Journal of Geophysical Research*, *103*(B8), 18,325–18,356. https://doi.org/10.1029/98JB00791

Michael, P. J., & Schilling, J.-G. (1989). Chlorine in mid-ocean ridge magmas: Evidence for assimilation of seawater-influenced components. *Geochimica et Cosmochimica Acta*, *53*(12), 3131–3143. https://doi.org/10.1016/0016-7037(89)90094-X

Nehlig, P. (1991). Salinity of oceanic hydrothermal fluids: A fluid inclusion study. *Earth and Planetary Science Letters*, *102*(3-4), 310–325. https://doi.org/10.1016/0012-821X(91)90026-E

Nehlig, P., Juteau, T., Bendel, V., & Cotten, J. (1994). The root zones of oceanic hydrothermal systems: Constraints from the Samail ophiolite (Oman). *Journal of Geophysical Research*, *99*(B3), 4703–4713. https://doi.org/10.1029/93JB02663

Nicolas, A., & Boudier, F. (1991). Rooting of the sheeted dike complex in the Oman ophiolite. In T. Peters, A. Nicolas & R. G. Coleman (Eds.), *Ophiolite genesis and evolution of the oceanic lithosphere* (pp. 39–54). Sultanate of Oman: Ministry of Petroleum and Minerals. https://doi.org/10.1007/978-94-011-3358-6_4

Nicolas, A., Boudier, F., Koepke, J., France, L., Ildefonse, B., & Mevel, C. (2008). Root zone of the sheeted dike complex in the Oman ophiolite. *Geochemistry, Geophysics, Geosystems*, *9*, Q05001. https://doi.org/10.1029/2007GC001918

Olive, J.-A., & Crone, T. J. (2018). Smoke without fire: How long can thermal cracking sustain hydrothermal circulation in the absence of magmatic heat? *Journal of Geophysical Research: Solid Earth*, *123*, 4561–4581. https://doi.org/10.1029/2017JB014900

Pallister, J. S., & Hopson, C. A. (1981). Samail ophiolite plutonic suite: Field relations, phase variation, cryptic variation and layering, and a model of a spreading ridge magma chamber. *Journal of Geophysical Research*, *86*(B4), 2593–2644. https://doi.org/10.1029/JB086iB04p02593

Pedersen, R. B. (1986). The nature and significance of magma chamber margins in ophiolites: Examples from the Norweigian Caledonides. *Earth and Planetary Science Letters*, *77*(1), 100–112. https://doi.org/10.1016/0012-821X(86)90136-6

Rosenberg, C. L., & Handy, M. R. (2005). Experimental deformation of partially melted granite revisited: Implications for the continental crust. *Journal of Metamorphic Geology*, *23*(1), 19–28. https://doi.org/10.1111/j.1525-1314.2005.00555.x

Rothery, D. A. (1983). The base of a sheeted dyke complex, Oman ophiolite: Implications for magma chambers at oceanic spreading axes. *Journal of the Geological Society*, *140*(2), 287–296. https://doi.org/10.1144/gsjgs.140.2.0287

Rushmer, T. (1996). Melt segregation in the lower crust: How have experiments helped us? *ransactions of the Royal Society of Edinburgh Earth Sciences*, *87*(1-2), 73–83. https://doi.org/10.1017/S0263593300006490

Saccocia, P., & Gillis, K. M. (1995). Hydrothermal upflow zones in the oceanic crust. *Earth and Planetary Science Letters*, *136*(1-2), 1–16. https://doi.org/10.1016/0012-821X(95)00155-5

Seyfried, W. E., Seewald, J. S., Berndt, M. E., Ding, K., & Foustoukos, D. I. (2003). Chemistry of hydrothermal vent fluids from the Main Endeavour Field, northern Juan de Fuca Ridge: Geochemical controls in the aftermath of June 1999 seismic events. *Journal of Geophysical Research*, *108*(B9), 2429. https://doi.org/10.1029/2002JB001957

Singh, S. C., Collier, J. S., Harding, A. J., Kent, G. M., & Orcutt, J. A. (1999). Seismic evidence for a hydrothermal layer above the solid roof of the axial magma chamber at the southern East Pacific Rise. *Geology*, *27*(3), 219–222. https://doi.org/10.1130/0091-7613(1999)027<0219:SEFAHL>2.3.CO;2

Sohn, R. A., Hildebrand, J. A., & Webb, S. C. (1999). A microearthquake survey of the high-temperature vent fields on the volcanically active East Pacific Rise (9°50'N). *Journal of Geophysical Research*, *104*(B11), 25367–25377. https://doi.org/10.1029/1999JB900263

Stakes, D. S., & Taylor, H. P. Jr. (1992). The Northern Samail Ophiolite: an oxygen isotope, microprobe and field study. *Journal of Geophysical Research*, *97*(B5), 7043–7080. https://doi.org/10.1029/91JB02743

Strens, M. R., & Cann, J. R. (1982). A model of hydrothermal circulation in fault zones at mid-ocean ridge crests. *Geophysical Journal of the Royal Astronomical Society*, *71*, 225-240.

Teagle, D. A. H., Alt, J. C., Umino, S., Miyashita, S., Banerjee, N. R., & Wilson, D. S. (2006). *Expedition 309/312 summary* (Vol. 309/312). College Station, TX: Ocean Drilling Program.

Teagle, D. A. H., Ildefonse, B., Blum, P., & Expedition scientists (2012). *Site 1256*, (Vol. 335). College Station, Texas: International Ocean Drilling Pogram Management International, Inc.

Tolstoy, M., Waldhauser, F., Bohnenstiehl, D. R., Weekly, R. T., & Kim, W. Y. (2008). Seismic identification of along-axis hydrothermal flow on the East Pacific rise. *Nature*, *451*(7175), 181–184. https://doi.org/10.1038/nature06424

Vigneresse, J. L., Barbey, P., & Cuney, M. (1996). Rheological transitions during partial melting and crystallization with application to felsic magma segregation and transfer. *Journal of Petrology*, *37*(6), 1579–1600. https://doi.org/10.1093/petrology/37.6.1579

Violay, M., Gibert, B., Mainprice, D., & Burg, J. P. (2015). Brittle versus ductile deformation as the main control of the deep fluid circulation in oceanic crust. *Geophysical Research Letters*, *42*, 2767–2773. https://doi.org/10.1002/2015GL063437

Violay, M., Gibert, B., Mainprice, D., Evans, B., Dautria, J. M., Azais, P., & Pezard, P. (2012). An experimental study of the brittle-ductile transition of basalt at oceanic crust pressure and temperature conditions. *Journal of Geophysical Research*, *117*, B03213. https://doi.org/10.1029/2011JB008884

Von Damm, K. L., & Lilley, M. D. (2004). Diffuse flow hydrothermal fluids from 9° 50′ N East Pacific Rise: Origin, evolution and biogeochemical controls. In W. S. Wilcock, E. F. Delong, D. S. Kelley, J. A. Baross, & S. C. Cary (Eds.), *The subseafloor biosphere at mid-ocean ridges* (Vol. 144, pp. 245-268)Washington, DC: American Geophysical Union.

Waldhauser, F., & Tolstoy, M. (2011). Seismogenic structure and processes associated with magma inflation and hydrothermal circulation beneath the East Pacific Rise at 9 degrees 50 ' N. *Geochemistry, Geophysics, Geosystems*, *12*, Q08T10. https://doi.org/10.1029/2011GC003568

Weekly, R. T., Wilcock, W. S. D., Toomey, D. R., Hooft, E. E. E., & Kim, E. (2014). Upper crustal seismic structure of the Endeavour segment, Juan de Fuca ridge from traveltime tomography: Implications for oceanic crustal accretion. *Geochemistry, Geophysics, Geosystems*, *15*, 1296–1315. https://doi.org/10.1002/2013GC005159

Wilcock, W. S. D., & Delaney, J. R. (1996). Mid-ocean ridge sulfide deposits: Evidence for heat extraction from magma chambers or cracking fronts? *Earth and Planetary Science Letters*, *145*(1-4), 49–64. https://doi.org/10.1016/S0012-821X(96)00195-1

Wilcock, W. S. D., Hooft, E. E. E., Toomey, D. R., McGill, P. R., Barclay, A. H., Stakes, D. S., & Ramirez, T. M. (2009). The role of magma injection in localizing black-smoker activity. *Nature Geoscience*, *2*(7), 509–513. https://doi.org/10.1038/ngeo550

Wilson, D. S., Teagle, D. A. H., Alt, J. C., Banerjee, N. R., Umino, S., Miyashita, S., Acton, G. D., et al. (2006). Drilling to gabbro in intact ocean crust. *Science*, *312*(5776), 1016–1020. https://doi.org/10.1126/science.1126090

Zhang, C., Koepke, J., Albrecht, M., Horn, I., & Holtz, F. (2017). Apatite in the dike-gabbro transition zone of mid-ocean ridge: Evidence for brine assimilation by axial melt lens. *American Mineralogist*, *102*(3), 558–570. https://doi.org/10.2138/am-2017-5906

Zhang, C., Koepke, J., France, L., & Godard, M. (2017). Felsic plutonic rocks from IODP Hole 1256D, Eastern Pacific: Implications for the nature of the axial melt lens at fast-spreading mid-ocean ridges. *Journal of Petrology*, *58*(8), 1535–1565. https://doi.org/10.1093/petrology/egx064